scientific reports

Check for updates

OPEN

Impact of Cattaneo-Christov heat flux model on MHD hybrid nano-micropolar fluid flow and heat transfer with viscous and joule dissipation effects

Asifa Tassaddiq

Review of literature reveals that hybrid nanofluids are more effective for heat transmission as compared to the conventional fluids. Nevertheless, the knowledge of developed techniques for the enhancement of heat transmission in hybrid nanofluids has many gaps and, subsequently, an extensive study for such fluids is vital. In this article, the author investigates the effect of hybrid nanoparticles on the thermal efficiency of nano-structured nanoparticles (micropolar fluid) by using the Cattaneo-Christov heat flux model. The magnetic field is pragmatic normal to the hybrid nanofluid flow direction. In order to investigate the influence of physical parameters, the proposed model has been converted to a set of ordinary differential equations (ODEs) by means of involved variables. Furthermore, the analytical and numerical approaches are compared by using different techniques to comprehend the significance of this research. It is found that macro-velocity field reduces with micropolar factor and Hartmann number. A significant result is found in micro-velocity field for the cases when $n = 0.5$ and $n = 0$. Also an escalating conduct in thermal field is observed against the increasing estimations of Hartmann number, micropolar parameter, Eckert number, and material parameter.

Abbreviations

A, d, a	Consistency parameters
B_0	Magnetic induction
c_p	Specific heat
C	Material parameter
Ec	Eckert number
Ha	Hartmann number
j	Length scale
k	Thermal conductivity
K	Micropolar parameter
n	Constant
Pr	Prandtl number
T	Temperature
T_w	Surface temperature
T_∞	Temperature outside from the surface
u, v	Velocity components
α, β, γ	Material parameters
Φ_1, Φ_2	Volume frictions
ψ	Stream function
σ	Electrical conductivity
ρ	Density

Department of Basic Sciences and Humanities, College of Computer and Information Sciences, Majmaah University, Al-Majmaah 11952, Saudi Arabia. email: a.tassaddiq@mu.edu.sa

γ	Spin gradient viscosity
κ	Thermal relaxation time

Subscripts

f	Fluid
nf	Nanofluid
hnf	Hybrid nanofluid

Enhancing the thermal transfer of operating nanoparticles by dispersing them has drawn as much scientific publicity as is evidenced by the fact that the distribution of nanomaterials enhances the operative thermal conductivity of these nanomaterials in which these nanoparticles are distributed. Theoretical and experimental research shows that functioning isolated fluids have comparatively poor thermal transfer capabilities compared to nanoparticle-containing fluids. Spectacular increase in the thermal efficiency of combinations consisting of nano-sized metallic particles has now been identified. After Choi's groundbreaking work[1], several scientists have performed experimental and theoretical analyses from diverse characteristics concerning the benefits of nanoparticles in thermal scheme. Nonetheless, some of the most recent and interconnected analysis have been identified. For instance, Dogonchi et al.[2] analyzed the function for the distribution of Fe_3O_4 in strengthening thermal transfer in the jar. They observed the consequences of thermal energy and the function of nanoparticles in the production of drugs throughout chemotherapy. Dogonchi and Hashim[3] deliberated the influence of Fe_3O_4 on the flow of water in a round tube. They even spoke about flow in a jar like such a rhombus. Various studies were implemented to examine the effect of magnetic dipole-dependent viscosity on just the transportation of energy in a nanofluid. Sheikholeslami et al.[4] formulated the transmission of phenomena in the porous medium subject to the magnetic field and developed computational formulations to explore the effect of nanoparticles on the energy transmission in water. Sheikholeslami and Rokni[5] explored the effect of the Coulomb force on the energy transportation in nanofluid through the cavity. Safaei et al.[6] have established computational models for the operation of hybrid nanomaterials in heat transmission to a permeable media that are subjected to imposed magnetic and have resolved formulated challenges to investigate the consequences of the resulting factors on the heat transmission. Safaei et al.[7] assessed the effect of ZnO-TiO on ethylene glycol thermal conductivity. Nadeem et al.[8] evaluated the effect of free-flow momentum on conduction in a water mixture containing Cu and Al_2O_3 under thermal slip procedure. Saleem et al.[9] carried out the study of the effect of thermal origin and viscous dissipation in nano-material released heat radiation. Sadiq et al.[10] conducted the simulations for the movement of the magnetic field linked through micropolar fluid and the nanoparticles dispersion. Other interrelated studies were published in[11–16]. The incompressible flow of hybrid dusty fluid using Darcian medium with Cattaneo-Christov model was discussed by Ganesh et al.[17]. In another article Reddy et al.[18] investigated the two-phase flow of Oldroyd-B fluid using Cattaneo-Christov model. Shah et al.[19–21] recently investigated the effects of heat transfer and thermal radiation on nanofluid flow in different geometries. Heat transfer features are studied with details in their work. Analytical and numerical approached are applied for the best solution of obtained modelled.

The flow of micropolar fluid initiated by Eringin[22] is concentrating presently. Ferrofluid, liquid crystals, blood, suspensions etc. are examples of micropolar fluid. The micropolar fluid theory presented by Eringin is built on continuum hypothesis. This theory states that those fluids which are composed of randomly oriented, rigid, or spherical particles with their specific microrotations or spins are known as micropolar fluids. The stagnation point micropolar fluid flow was determined by Guram and smith[23]. The micropolar fluid flow over axisymmetric sheets with heat source was investigated by Gorla and Takhar[24]. The stagnation flow of micropolar fluid with combine convective conditions was presented by Gorla et al.[25]. Sedeek[26] probed the micropolar fluid flow past a moving sheet with magnetic field influence by means of micropolar fluid theory. Nazar et al.[27] determined the stagnation point of a micropolar viscous fluid flow. The micropolar fluid flow and heat transmission by means of finite element technique was discussed by Takhar et al.[28]. The heat transmission in a micropolar fluid flow in a porous media was addressed by Eldahab et al.[29]. Nazar et al.[30] scrutinized the boundary layer flow of micropolar fluid on a sphere. For more understanding and analysis of the relevant nano fluid flow, the interested reader is referred to recent researches[31–39].

By means of a systematic review, the researchers have found that the analysis (using HAM and Shooting) on the consequence of hybrid nanoparticles on the thermal efficiency of nano-structured nanoparticles (micropolar fluid) has not yet been performed. The Cattaneo-Christov heat flux model is performed in the current investigation. This research will fill this space in current scientific innovations. The present research problem is solved analytically and numerically as well. The results obtained are presented graphically and discussed briefly.

Problem formulation

Here it is assumed the micropolar fluid flow over an elastic body with Cattaneo-Christov heat flux model conditional on dispersion of hybrid nanoparticles Cu and Al_2O_3. The elastic body is moving with velocity $U_w(x) = ax$. The temperature of the stretchable body is taken as $T_w(x) > T$ where T and T_w is the fluid's temperature and the stretchable surface's temperature of the elastic body. The magnetic field $B = \left[0,\ AB_0x^{-1},\ 0\right]$ is practiced vertical to the fluid flow as shown in Fig. 1.

$$\frac{\partial u}{\partial x} + \frac{\partial v}{\partial y} = 0, \tag{1}$$

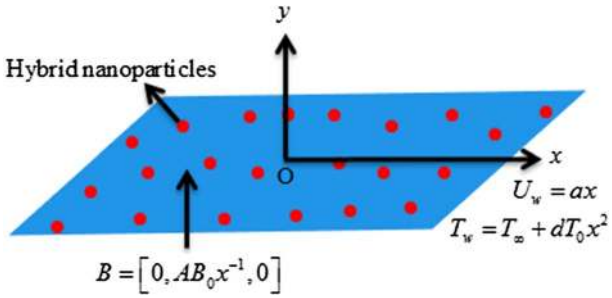

Figure 1. Fluid flow geometry.

$$u\frac{\partial u}{\partial x} + v\frac{\partial u}{\partial y} = \frac{1}{\rho_{hnf}}\left(\mu_{hnf} + \lambda_{hnf}\right)\frac{\partial^2 u}{\partial y^2} - \frac{\sigma_{hnf}A^2B_0^2x^{-2}}{\rho_{hnf}}u - \frac{\lambda_{hnf}}{\rho_{hnf}}\frac{\partial N}{\partial y}, \tag{2}$$

$$\rho_{hnf}j\left(u\frac{\partial N}{\partial x} + v\frac{\partial N}{\partial y}\right) = \gamma_{hnf}\frac{\partial^2 N}{\partial y^2} - \lambda_{hnf}\left(2N + \frac{\partial u}{\partial y}\right), \tag{3}$$

$$\begin{aligned}\left(\rho c_p\right)_{hnf}\left(u\frac{\partial T}{\partial x} + v\frac{\partial T}{\partial y}\right) &= k_{hnf}\frac{\partial^2 T}{\partial y^2} + \sigma_{hnf}A^2B_0^2x^{-2}u^2 + \left(\mu_{hnf} + \frac{\lambda_{hnf}}{2}\right)\left(\frac{\partial u}{\partial y}\right)^2 \\ &\quad - \lambda_1\begin{pmatrix} u\frac{\partial T}{\partial x}\frac{\partial u}{\partial x} + u\frac{\partial T}{\partial y}\frac{\partial v}{\partial x} + v\frac{\partial T}{\partial y}\frac{\partial v}{\partial y} + v\frac{\partial T}{\partial x}\frac{\partial u}{\partial y} \\ +2vu\frac{\partial^2 T}{\partial x\partial y} + u^2\frac{\partial^2 T}{\partial x^2} + v^2\frac{\partial^2 T}{\partial y^2}\end{pmatrix} \\ &\quad + \frac{\lambda_{hnf}}{2}\left(\frac{\partial u}{\partial y} - 2N\right)^2 + (\alpha+\beta+\gamma)\left(\frac{\partial N}{\partial y}\right)^2,\end{aligned} \tag{4}$$

With

$$\begin{aligned} &u = U_w x,\ v = 0,\ T = T_w,\ N = -n\frac{\partial u}{\partial y}\ \text{ at }\ y = 0, \\ &u \to 0,\ \ T \to T_\infty,\ \ N \to 0\ \ as\ \ y \to \infty. \end{aligned} \tag{5}$$

Here n represents the constant lies in [0 1]. For the situation when micro-motion disappears at the surface i.e. $n = 0$. For the situation when micro-motion not disappears at the surface, the constant i.e. $n = 0.5$, and $n = 1$ is for the situation of turbulent flow.

The thermo-physical properties used in the modeled problem are defined by

$$\begin{aligned} \frac{\rho_{hnf}}{\rho_f} &= (1-\Phi_2)\left\{1 - \Phi_1 + \Phi_1\frac{\rho_{S1}}{\rho_f}\right\} + \Phi_2\frac{\rho_{S2}}{\rho_f},\ \ \mu_{hnf} = \frac{\mu_f}{(1-\Phi_1)^{5/2}(1-\Phi_2)^{5/2}}, \\ \frac{\left(\rho c_p\right)_{hnf}}{\left(\rho c_p\right)_f} &= (1-\Phi_2)\left\{1 - \Phi_1 + \Phi_1\frac{\left(\rho c_p\right)_{S1}}{\left(\rho c_p\right)_f}\right\} + \Phi_2\frac{\left(\rho c_p\right)_{S2}}{\left(\rho c_p\right)_f},\ \ \lambda_{hnf} = \frac{\lambda_f}{(1-\Phi_1)^{5/2}(1-\Phi_2)^{5/2}}, \\ \frac{k_{hnf}}{k_{bf}} &= \frac{2k_{bf} + k_{S2} - 2\Phi_2\left(k_{bf} - k_{S2}\right)}{2k_{bf} + k_{S2} + \Phi_2\left(k_{bf} - k_{S2}\right)},\ \ \frac{k_{bf}}{k_f} = \frac{2k_f + k_{S1} - 2\Phi_1\left(k_f - k_{S1}\right)}{2k_f + k_{S1} + \Phi_1\left(k_f - k_{S1}\right)}, \\ \frac{\sigma_{hnf}}{\sigma_{bf}} &= \frac{2\sigma_{bf} + \sigma_{S2} - 2\Phi_2\left(\sigma_{bf} - \sigma_{S2}\right)}{2\sigma_{bf} + \sigma_{S2} + \Phi_2\left(\sigma_{bf} - \sigma_{S2}\right)},\ \ \frac{\sigma_{bf}}{\sigma_f} = \frac{2\sigma_f + \sigma_{S1} - 2\Phi_1\left(\sigma_f - \sigma_{S1}\right)}{2\sigma_f + \sigma_{S1} + \Phi_1\left(\sigma_f - \sigma_{S1}\right)}. \end{aligned} \tag{6}$$

Here, the subscripts $S1$ and $S2$ are used for Cu and Al_2O_3 nanoparticles respectively. The nano-particles' thermo-physical properties and micro polar fluid are displayed in Table 1.

The similarity variables are defined by

$$\begin{aligned} u &= \frac{\partial\psi}{\partial y},\ \ v = -\frac{\partial\psi}{\partial x},\ \ \psi(x,y) = \left(a\upsilon_f\right)^{1/2}xf(\xi), \\ \theta(\xi) &= \frac{T - T_\infty}{T_w - T_\infty},\ \ N(\xi) = x\left(\frac{a^3}{\upsilon_f}\right)^{1/2}g(\xi),\ \ \xi = \left(\frac{a}{\upsilon_f}\right)^{1/2}y. \end{aligned} \tag{7}$$

Physical property	Cu	Al_2O_3	Blood
$\rho/(\mathrm{kg\ m^{-3}})$	8933	3970	1060
$c_p/\left(\mathrm{J\ kg^{-1}K^{-1}}\right)$	385	765	3770
$k/(\mathrm{W\ m^{-1}K^{-1}})$	401	40	40
Φ	0.05	0.15	0.0
$\sigma/(\mathrm{s\ m^{-1}})$	59.6×10^6	35×10^6	4.3×10^{-5}

Table 1. The nano-particles' thermo-physical properties and micro polar fluid.

On substituting (7) in (2–5), we have

$$\begin{aligned}&(1+K)f'''+Kg'+\frac{\sigma_{hnf}}{\sigma_f\left[(1-\Phi_2)\left\{1-\Phi_1+\Phi_1\frac{\rho_{S1}}{\rho_f}\right\}+\Phi_2\frac{\rho_{S2}}{\rho_f}\right]}Haf'\\&-(1-\Phi_1)^{2.5}(1-\Phi_2)^{2.5}\left[(1-\Phi_2)\left\{1-\Phi_1+\Phi_1\frac{\rho_{S1}}{\rho_f}\right\}+\Phi_2\frac{\rho_{S2}}{\rho_f}\right]\left(f'^2-ff''\right)=0,\end{aligned}\tag{8}$$

$$\left(1+\frac{K}{2}\right)g''-K\left(2g+f''\right)-(1-\Phi_1)^{2.5}(1-\Phi_2)^{2.5}\left[(1-\Phi_2)\left\{\begin{matrix}1-\Phi_1+\\\Phi_1\frac{\rho_{S1}}{\rho_f}\end{matrix}\right\}+\Phi_2\frac{\rho_{S2}}{\rho_f}\right]\left(f'g-fg'\right)=0,\tag{9}$$

$$\begin{aligned}&\frac{k_{hnf}}{k_f}\theta''+\frac{\sigma_{hnf}}{\sigma_f}Ha\,\mathrm{Pr}\,Ecf'^2+\left(1+\frac{K}{2}\right)\frac{Ec\,\mathrm{Pr}}{(1-\Phi_1)^{2.5}(1-\Phi_2)^{2.5}}f''^2\\&+\frac{K}{2}\frac{Ec\,\mathrm{Pr}}{(1-\Phi_1)^{2.5}(1-\Phi_2)^{2.5}}\left(f''^2+4g^2-4gf''\right)+CEc\,\mathrm{Pr}\,\mathrm{Re}g'^2-\kappa\left(ff'\theta'+f^2\theta''\right)\\&+\mathrm{Pr}\left[(1-\Phi_2)\left\{1-\Phi_1+\Phi_1\frac{(\rho c_p)_{S1}}{(\rho c_p)_f}\right\}+\Phi_2\frac{(\rho c_p)_{S2}}{(\rho c_p)_f}\right]\left(f\theta'-f'\theta\right)=0,\end{aligned}\tag{10}$$

$$\begin{aligned}&f=0,f'=1,g'=-nf'',\theta=1,\quad\text{at}\ \xi=0\\&f'=0,\ g'=0,\theta=0\quad\text{as}\ \xi\to\infty.\end{aligned}\tag{11}$$

The dimensionless variables are defined as

$$\begin{aligned}&Ha=\frac{\sigma_f A^2B_0^2x^2}{a\rho_f},\quad K=\frac{\lambda_f}{\mu_f},\quad \mathrm{Pr}=\frac{\mu_f\left(c\rho_p\right)_f}{k_f},\quad \kappa=\lambda a,\\&Ec=\frac{a^2x^2}{(T_w-T_\infty)\left(c_p\right)_f},\quad \mathrm{Re}=\frac{ax^2}{\upsilon_f},\quad C=\frac{(\alpha+\beta+\gamma)}{x^2\mu_f},\end{aligned}\tag{12}$$

where Ha indicates the Hartmann number, K represents the micropolar parameter, Pr signifies the Prandtl number, Ec represents the Eckert number,Re indicates the Reynolds number, C represents the material parameter, and κ signifies the thermal relaxation parameter.

$$\begin{aligned}C_f&=\frac{1+\frac{K}{2}}{(\mathrm{Re})^{1/2}(1-\Phi_1)^{2.5}(1-\Phi_2)^{2.5}}f''(0),\\C_g&=\frac{1+\frac{K}{2}}{(\mathrm{Re})^{1/2}(1-\Phi_1)^{2.5}(1-\Phi_2)^{2.5}}g'(0),\\Nu&=-(\mathrm{Re})^{1/2}\frac{k_{hnf}}{k_f}\theta'(0).\end{aligned}\tag{13}$$

Analytical solution

To proceed the modeled equations by using HAM, we assumed that $f=F,\ g=G,\ \theta=T$ and $\xi=\psi$. In understanding of (8–10) with (11), HAM is used with the following procedure.

Preliminary assumptions

$$F_0(\psi)=1-e^{-\psi},\ G_0(\psi)=-ne^{-\psi},\ T_0(\psi)=e^{-\psi}.\tag{14}$$

Linear operators

$$L_F(F) = \left(F''' - F'\right),\ \mathrm{L}_G(G) = \left(G'' - G\right),\ \mathrm{L}_T(T) = \left(T'' - T\right), \tag{15}$$

with

$$L_F\left(p_1 + p_2 e^{-\psi} + p_3 e^{\psi}\right) = 0,\ \mathrm{L}_G\left(p_4 e^{-\psi} + p_5 e^{\psi}\right) = 0, \mathrm{L}_T\left(p_6 e^{-\psi} + p_7 e^{\psi}\right) = 0. \tag{16}$$

where $p_i (i = 1 - 7)$ are constants in general solution.

0th-order problems

Assume that $S \in [0,\ 1]$ be the rooted factor and h_F, h_G and h_T are the non-zero auxiliary factors. then 0th-order problems are

$$(1 - S)L_F[F(\psi; S) - F_0(\psi)] = S\hbar_F \aleph_F[F(\psi; S), F(\psi; S)], \tag{17}$$

$$(1 - S)L_G[G(\psi; S) - G_0(\psi)] = S\hbar_G \aleph_G[G(\psi; S), F(\psi; S)], \tag{18}$$

$$(1 - S)L_T[T(\psi; S) - T_0(\psi)] = S\hbar_T \aleph_T[T(\psi; S), F(\psi; S), G(\psi; S)], \tag{19}$$

$$\begin{aligned} &F(0; S) = 0,\ \ F'(0; S) = 1,\ \ G'(0; S) = -nF''(0; S),\ \ T(0; S) = 1, \\ &F'(\infty; S) = 0,\ \ G'(\infty; S) = 0,\ \ T(\infty; S) = 0\,. \end{aligned} \tag{20}$$

$$\begin{aligned} \aleph_F\left[F(\psi; S), g(\psi; S)\right] &= (1 + K)\frac{\partial^3 F(\psi; S)}{\partial \psi^3} + K\frac{\partial G(\psi; S)}{\partial \psi} \\ &+ \frac{\sigma_{hnf}}{\sigma_f\left[(1 - \Phi_2)\left\{1 - \Phi_1 + \Phi_1\frac{\rho_{S1}}{\rho_f}\right\} + \Phi_2\frac{\rho_{S2}}{\rho_f}\right]} Ha\frac{\partial F(\psi; S)}{\partial \psi} \\ &-(1 - \Phi_1)^{2.5}(1 - \Phi_2)^{2.5}\left[(1 - \Phi_2)\left\{\begin{matrix}1 - \Phi_1 \\ +\Phi_1\frac{\rho_{S1}}{\rho_f}\end{matrix}\right\} + \Phi_2\frac{\rho_{S2}}{\rho_f}\right]\left(\begin{matrix}\left(\frac{\partial F(\psi; S)}{\partial \psi}\right)^2 \\ -F(\psi; S)\frac{\partial^2 F(\psi; S)}{\partial \psi^2}\end{matrix}\right), \end{aligned} \tag{21}$$

$$\begin{aligned} \aleph_G[G(\psi; S), F(\psi; S)] &= \left(1 + \frac{K}{2}\right)\frac{\partial^2 G(\psi; S)}{\partial \psi^2} - K\left(2G(\psi; S) + \frac{\partial^2 F(\psi; S)}{\partial \psi^2}\right) \\ &-(1 - \Phi_1)^{2.5}(1 - \Phi_2)^{2.5}\left[(1 - \Phi_2)\left\{1 - \Phi_1 + \Phi_1\frac{\rho_{S1}}{\rho_f}\right\} + \Phi_2\frac{\rho_{S2}}{\rho_f}\right] \\ &\left(\frac{\partial F(\psi; S)}{\partial \psi}G(\psi; S) - F(\psi; S)\frac{\partial F(\psi; S)}{\partial \psi}\right), \end{aligned} \tag{22}$$

$$\begin{aligned} \aleph_T[T(\psi; S), F(\psi; S), G(\psi; S)] &= \frac{k_{hnf}}{k_f}\frac{\partial^2 T(\psi; S)}{\partial \psi^2} + \left(1 + \frac{K}{2}\right)\frac{Ec\,\mathrm{Pr}}{(1 - \Phi_1)^{2.5}(1 - \Phi_2)^{2.5}} \\ &\left(\frac{\partial^2 F(\psi; S)}{\partial \psi^2}\right)^2 + \frac{K}{2}\frac{Ec\,\mathrm{Pr}}{(1 - \Phi_1)^{2.5}(1 - \Phi_2)^{2.5}}\left(\begin{matrix}\left(\frac{\partial^2 F(\psi; S)}{\partial \psi^2}\right)^2 + 4(G(\psi; S))^2 \\ -4G(\psi; S)\frac{\partial^2 F(\psi; S)}{\partial \psi^2}\end{matrix}\right) \\ &+CEc\,\mathrm{Pr}\,\mathrm{Re}\left(\frac{\partial G(\psi; S)}{\partial \psi}\right)^2 + \mathrm{Pr}\left[(1 - \Phi_2)\left\{1 - \Phi_1 + \Phi_1\frac{(\rho c_p)_{S1}}{(\rho c_p)_f}\right\} + \Phi_2\frac{(\rho c_p)_{S2}}{(\rho c_p)_f}\right] \\ &\left(F(\psi; S)\frac{\partial T(\psi; S)}{\partial \psi} - \frac{\partial F(\psi; S)}{\partial \psi}T(\psi; S)\right) - \kappa\left(F(\psi; S)\frac{\partial F(\psi; S)}{\partial \psi}\frac{\partial T(\psi; S)}{\partial \psi}\right. \\ &\left.+(F(\psi; S))^2\frac{\partial^2 T(\psi; S)}{\partial \psi^2}\right) + \frac{\sigma_{hnf}}{\sigma_f}Ha\,\mathrm{Pr}\,Ec\left(\frac{\partial F(\psi; S)}{\partial \psi}\right)^2, \end{aligned} \tag{23}$$

*k*th-*order problems*

*k*th-order problems are

$$L_F[F_k(\psi) - \chi_k F_{k-1}(\psi)] = \hbar_k \Re_k^F(\psi), \tag{24}$$

$$L_G[G_k(\psi) - \chi_k G_{k-1}(\psi)] = \hbar_k \Re_k^G(\psi), \tag{25}$$

$$L_T[T_k(\psi) - \chi_k T_{k-1}(\psi)] = \hbar_T \Re_k^T(\psi), \tag{26}$$

$$F_k(0) = F_k'(0) = G_k'(0) = T_k(0) = F_k'(\infty) = G_k'(\infty) = T_k(\infty) = 0. \tag{27}$$

$$\begin{aligned}\Re_k^F(\psi) &= (1+K)F_{k-1}''' + KG_{k-1}' + \frac{\sigma_{hnf}}{\sigma_f\left[(1-\Phi_2)\left\{1-\Phi_1+\Phi_1\frac{\rho_{S1}}{\rho_f}\right\}+\Phi_2\frac{\rho_{S2}}{\rho_f}\right]}HaF_{k-1}' \\ &-(1-\Phi_1)^{2.5}(1-\Phi_2)^{2.5}\left[(1-\Phi_2)\left\{1-\Phi_1+\Phi_1\frac{\rho_{S1}}{\rho_f}\right\}+\Phi_2\frac{\rho_{S2}}{\rho_f}\right]\left(F_{k-1}'^2 - \sum_{j=0}^{k-1}\left(F_{k-1-j}F_{k-1}''\right)\right),\end{aligned} \tag{28}$$

$$\begin{aligned}\Re_k^G(\psi) &= \left(1+\frac{K}{2}\right)G_{k-1}'' - K\left(2G_{k-1}+F_{k-1}''\right) \\ &-(1-\Phi_1)^{2.5}(1-\Phi_2)^{2.5}\left[(1-\Phi_2)\left\{1-\Phi_1+\Phi_1\frac{\rho_{S1}}{\rho_f}\right\}+\Phi_2\frac{\rho_{S2}}{\rho_f}\right]\left(\sum_{j=0}^{k-1}\left(F_{k-1-j}'G_{k-1}\right) - \sum_{j=0}^{k-1}\left(F_{k-1-j}G_{k-1}'\right)\right),\end{aligned} \tag{29}$$

$$\begin{aligned}\Re_k^T(\psi) &= \frac{k_{hnf}}{k_f}T_{k-1}'' + \frac{\sigma_{hnf}}{\sigma_f}Ha\,\mathrm{Pr}\,EcF_{k-1}'^2 + \left(1+\frac{K}{2}\right)\frac{Ec\,\mathrm{Pr}}{(1-\Phi_1)^{2.5}(1-\Phi_2)^{2.5}}F_{k-1}''^2 \\ &+\frac{K}{2}\frac{Ec\,\mathrm{Pr}}{(1-\Phi_1)^{2.5}(1-\Phi_2)^{2.5}}\left(F_{k-1}''^2 + 4G_{k-1}^2 - 4\sum_{j=0}^{k-1}\left(G_{k-1-j}F_{k-1}''\right)\right) + CEc\,\mathrm{Pr}\,\mathrm{Re}G_{k-1}'^2 \\ &+\mathrm{Pr}\left[(1-\Phi_2)\left\{1-\Phi_1+\Phi_1\frac{(\rho c_p)_{S1}}{(\rho c_p)_f}\right\}+\Phi_2\frac{(\rho c_p)_{S2}}{(\rho c_p)_f}\right]\left(\sum_{j=0}^{k-1}\left(F_{k-1-j}T_{k-1}'\right) - \sum_{j=0}^{k-1}\left(F_{k-1-j}'T_{k-1}\right)\right) \\ &-\kappa\left(\sum_{j=0}^{k-1}\left(F_{k-1-j}F_{k-1}'T_k'\right) + \sum_{j=0}^{k-1}\left(F_{k-1-j}^2T_{k-1}''\right)\right).\end{aligned} \tag{30}$$

When $S = 0$ and $S = 1$, we can write

$$F(\psi;0) = F_0(\psi), \quad F(\psi;1) = F(\psi), \tag{31}$$

$$G(\psi;0) = G_0(\psi), \quad G(\psi;1) = G(\psi), \tag{32}$$

$$T(\psi;0) = T_0(\psi), \quad T(\psi;1) = T(\psi), \tag{33}$$

when S fluctuates from 0 to 1, the results varies from initial to final solutions. By Taylor's series expansion

$$F(\psi;S) = F_0(\psi) + \sum_{k=1}^{\infty}F_k(\psi)S^k, \quad F_k = \frac{1}{k!}\frac{\partial^k F(\psi;S)}{\partial S^k}\bigg|_{S=0}, \tag{34}$$

$$G(\psi;S) = G_0(\psi) + \sum_{k=1}^{\infty}G_k(\psi)S^k, \quad G_k = \frac{1}{k!}\frac{\partial^k G(\psi;S)}{\partial S^k}\bigg|_{S=0}, \tag{35}$$

$$T(\psi;S) = T_0(\psi) + \sum_{k=1}^{\infty}T_k(\psi)S^k, \quad T_k = \frac{1}{k!}\frac{\partial^k T(\psi;S)}{\partial S^k}\bigg|_{S=0}. \tag{36}$$

The series (34) and (36) converge at $S = 1$, that is

$$F(\psi) = F_0(\psi) + \sum_{k=1}^{\infty}F_k(\psi), \tag{37}$$

$$G(\psi) = G_0(\psi) + \sum_{k=1}^{\infty}G_k(\psi), \tag{38}$$

$$T(\psi) = T_0(\psi) + \sum_{k=1}^{\infty}T_k(\psi), \tag{39}$$

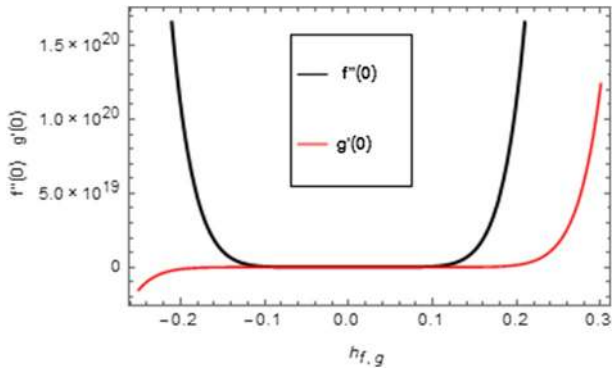

Figure 2. $\hbar$-curves for velocity field and micro-rotation field.

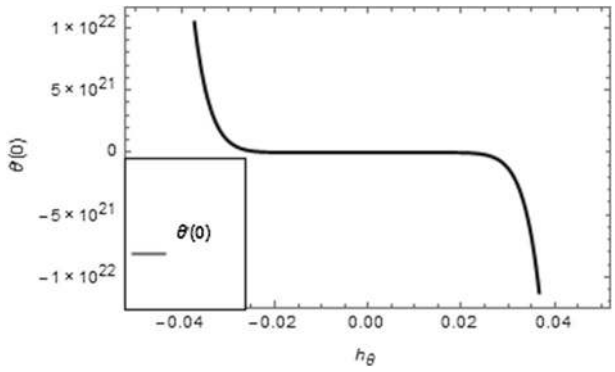

Figure 3. $\hbar$-curve for temperature field.

where

$$\chi_k = \begin{cases} 0, & k \leq 1, \\ 1, & k > 1. \end{cases} \tag{40}$$

Convergence solution

The supplementary factors $\hbar_f$, $\hbar_g$ and $\hbar_\theta$ convoluted in the series solutions for velocity, micro-rotation, and temperature fields of hybrid nanofluid are characterized as convergence regulator factors. These factors are used to stabilize the convergence of the demonstrated problem. The suitable standards of the $\hbar_f$, $\hbar_g$ and $\hbar_\theta$ are $-0.15 \leq \hbar_f \leq 0.15, -0.2 \leq \hbar_g \leq 0.22$ and $-0.03 \leq \hbar_\theta \leq 0.03$ which are shown in Figs. 2 and 3.

Analytical and numerical comparison

Association between analytical and numerical procedures for velocity, micro-rotation and thermal fields are presented here. Both the procedures are preserved with the conventional computer programs and authenticated by reproducing the consequences to the manageable standard and have totaled with mathematica software. Figure 4 specifies the assessment of HAM and shooting methods for velocity field $f'(\xi)$. Similarly Figs. 5 and 6 denote the assessment of HAM and shooting methods for micro-rotation field $g(\xi)$ and thermal field $\theta(\xi)$, respectively. Also Table 2 is displayed for the assessment of HAM and shooting procedures.

Results and discussion

This segment deals with the physical impact of constraints on the nanofluid (Al_2O_3) and hybrid nanofluid (Al_2O_3, Cu) flows when, $\Pr = 2.3$, $Ha = 1.5$, $Ec = 0.5$, $\kappa = 1.0$, $K = 0.6$, and $C = 0.3$. These impacts are displayed in Figs. 7, 8, 9, 10, 11, 12, 13, 14, 15, 16. The deviation in velocity field contrasted with Hartmann number is depicted in Fig. 7. As the estimations of Hartmann number intensifies, the boundary layer thickness of the velocity field escalates. This is attributable to the datum that the existence of a Hartmann number is measured by the Lorentz force, so throughout a delaying force is conceived throughout the velocity field. Thus as the estimations of Ha grows, so is the restricting force and thus the velocity field declines. The contrary impression of Hartmann number on temperature field is observed in Fig. 8. It is found that as the estimations of Ha increase, the temperature at the surface and the thermal boundary layer thickness declines. The variation in velocity field against micropolar fluid parameter is displayed in Fig. 9. It is remarkable to know that $n = 0$ is the situation when

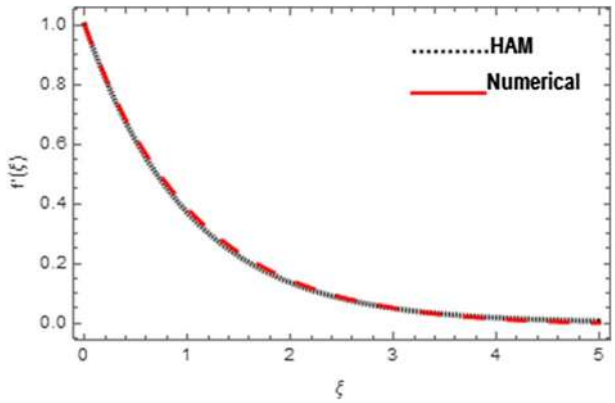

Figure 4. Association between HAM and Shooting techniques for velocity field.

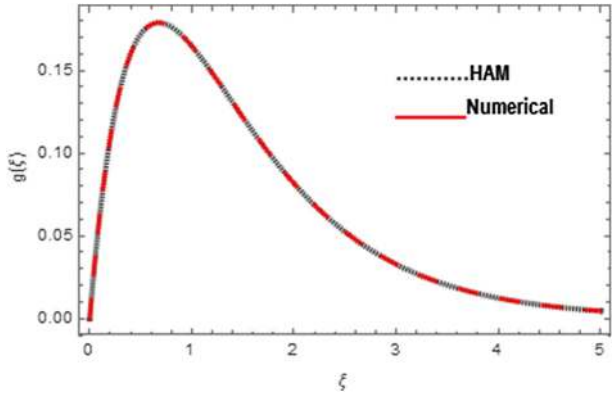

Figure 5. Association between HAM and Shooting techniques for microrotation field.

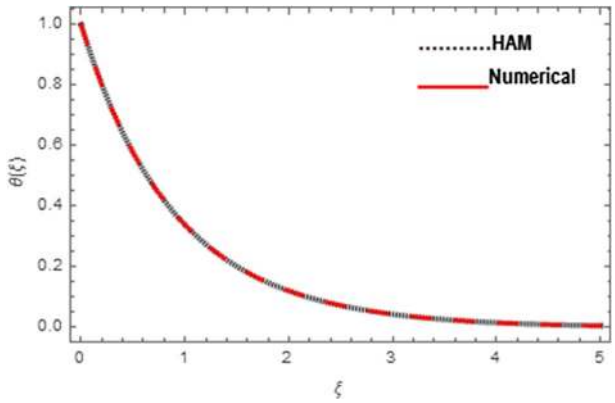

Figure 6. Association between HAM and Shooting techniques for temperature field.

the motion of the nanofluid and hybrid nanoparticles disappears at the surface of the body. It is depicted here that higher estimations of micropolar fluid parameter declines the velocity field of the flow. It is furthermore important and well-known here that the boundary layer thickness is smaller for the hybrid nanofluid than that of nanofluid. Figures 10 and 11 exhibit the variation in micro-rotation field against micropolar fluid parameter for the situations when $n = 0.5$ and $n = 0$, respectively. For the case when $n = 0.5$, the micro-rotation field declines with the higher estimations of micropolar fluid parameter. This deviation is publicized in Fig. 10. For the case when $n = 0$, the micro-rotation field exhibits the diverse impression with escalation in micropolar fluid parameter. This effect is shown in Fig. 11. An increasing behavior in thermal field with the escalating estimations of micropolar fluid parameter is displayed in Fig. 12. Physically, the rise in micropolar fluid parameter enables heightening in thermal boundary layer thickness, and thus the thermal field enhances. The relation of the thermal

	Velocity field		Micro-rotation field		Temperature field	
ξ	HAM	Shooting	HAM	Shooting	HAM	Shooting
0.0	-7.5×10^{-19}	0.000000	-3.53×10^{-9}	0.000000	-3.97×10^{-9}	0.000000
0.5	0.393940	0.397855	0.523062	0.514206	0.599470	0.599799
1.0	0.633330	0.644735	0.372430	0.364476	0.361400	0.361695
1.5	0.778692	0.797385	0.246020	0.239908	0.218506	0.218717
2.0	0.866920	0.891134	0.156424	0.152343	0.132305	0.132444
2.5	0.920454	0.948022	0.097504	0.094893	0.080171	0.080258
3.0	0.952933	0.981823	0.060101	0.058468	0.048600	0.048654
3.5	0.972663	1.001170	0.036806	0.035797	0.029468	0.029501
4.0	0.984587	1.011490	0.022453	0.021835	0.017870	0.017890
4.5	0.991836	1.016185	0.013666	0.013289	0.010837	0.010849
5.0	0.996233	1.017429	0.008306	0.008076	0.006572	0.006580

Table 2. Numerical association between HAM and Shooting techniques for velocity, micro-rotation, and temperature fields.

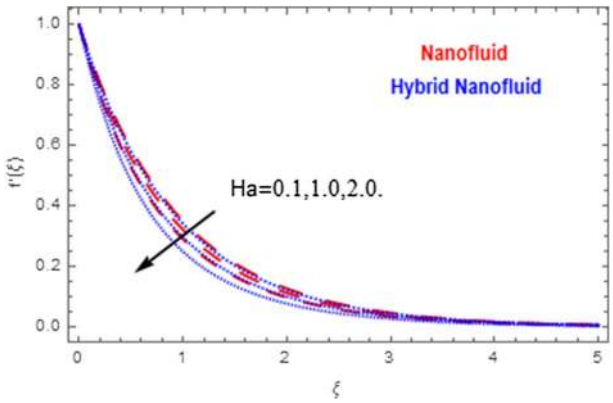

Figure 7. Variation in velocity field of nanofluid (Al_2O_3) and hybrid nanofluid (Al_2O_3, Cu) against different estimations of *Ha*.

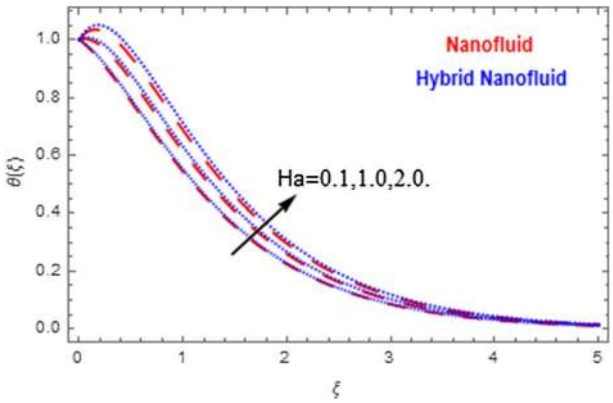

Figure 8. Variation in temperature field of nanofluid (Al_2O_3) and hybrid nanofluid (Al_2O_3, Cu) against different estimations of *Ha*.

field versus relaxation time parameter κ is depicted in Fig. 13. The temperature relaxation time factor decreases the thermal profile and the related thermal boundary layer thickness. Actually, this demonstrates that the gradual existence of κ takes additional time to change the energy from tightly loaded fluid particles to lower active flow particles. It demonstrates a representation of the features of non-conductive fluid material. The Influence of Eckert number on thermal field of the nanofluid and hybrid nanofluid is put on a display in Fig. 14. The heightening

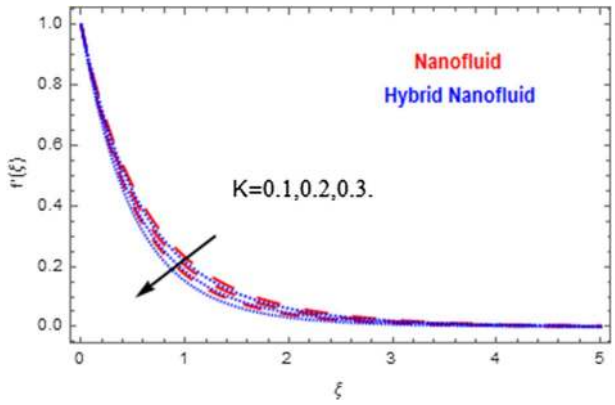

Figure 9. Variation in velocity field of nanofluid (Al_2O_3) and hybrid nanofluid (Al_2O_3, Cu) against different estimations of K.

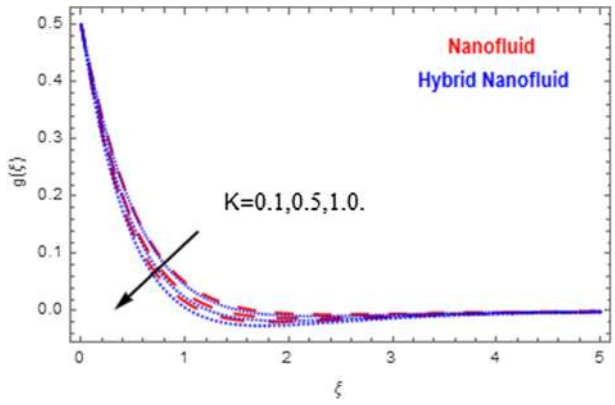

Figure 10. Variation in microrotation field of nanofluid (Al_2O_3) and hybrid nanofluid (Al_2O_3, Cu) against different estimations of K when $n = 0.5$.

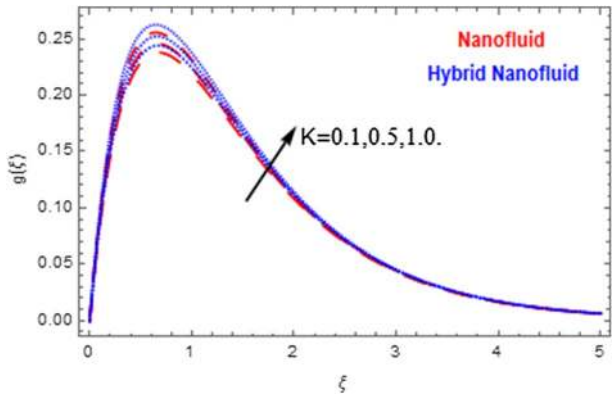

Figure 11. Variation in microrotation field of nanofluid (Al_2O_3) and hybrid nanofluid (Al_2O_3, Cu) against different estimations of K when $n = 0$.

Eckert number heightens the thermal field. In the case of a large magnetic force system, the major disruption of the temperature field induced by each member is an interesting result. Such physical phenomena are attributable to the cumulative effect heat energy stored in the nanofluid and hybrid nanofluid due to fractional heating. The variation in thermal field against material parameter is displayed in Fig. 15. An increasing impact is seen here. The higher estimations of material parameter raise the thermal field of the nanofuid and hybrid nanofluid. The variation in thermal field of the nanofluid and hybrid nanofluid versus Prandtl number Pr is displayed in Fig. 16.

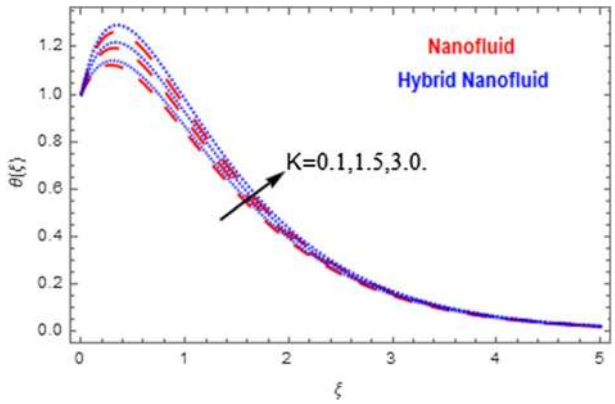

Figure 12. Variation in temperature field of nanofluid (Al_2O_3) and hybrid nanofluid (Al_2O_3, Cu) against different estimations of K.

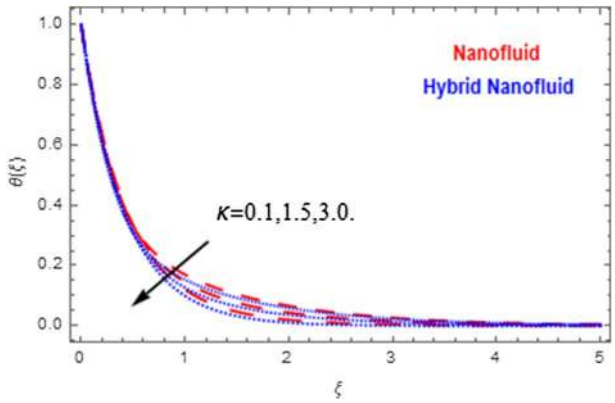

Figure 13. Variation in temperature field of nanofluid (Al_2O_3) and hybrid nanofluid (Al_2O_3, Cu) against different estimations of κ.

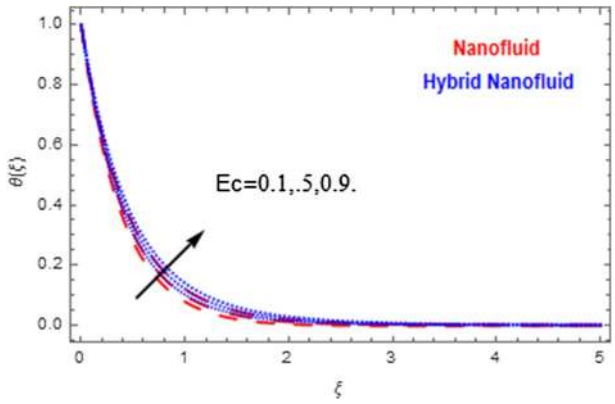

Figure 14. Variation in temperature field of nanofluid (Al_2O_3) and hybrid nanofluid (Al_2O_3, Cu) against different estimations of Ec.

The graph shows that thermal field and thermal layer thickness decline whenever the Pr values boost. This really is caused by the fact that the greater number of Prandtl, fluids will have a comparatively low conductivity, that mostly diminishes the heat transfer and the thickness of the thermal fluid flow and therefore the temperature of the fluid reduces. Growing Pr is an improvement in the thermal transfer rate on the surface, even though the

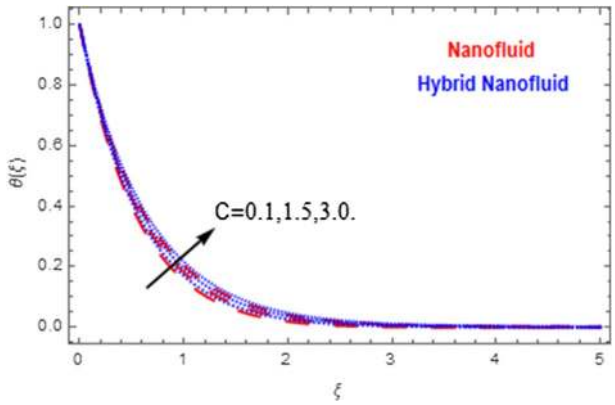

Figure 15. Variation in temperature field of nanofluid (Al_2O_3) and hybrid nanofluid (Al_2O_3, $CuAl_2O_3$, Cu) against different estimations of C.

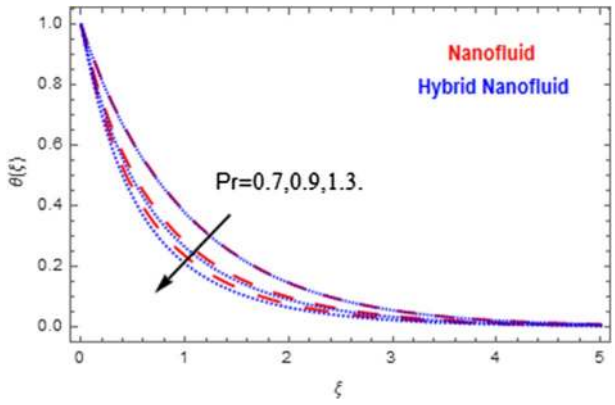

Figure 16. Variation in temperature field of nanofluid (Al_2O_3) and hybrid nanofluid (Al_2O_3, Cu) against different estimations of Pr.

Nanofluid				Hybrid nanofluid		
	C_f	C_g	Nu	C_f	C_gC_g	Nu
K	$n = 0.5$			$n = 0.5$		
0.0	1.116551	4.984882	1.454353	0.845883	3.776366	1.632642
0.8	2.427641	9.040594	1.253680	1.682611	6.383817	1.425742
1.5	3.364413	12.343846	1.158973	2.283628	8.560773	1.379473
2.0	3.947586	14.656566	1.126438	2.661480	10.092277	1.356843
	C_f	C_g	Nu	C_f	C_g	Nu
K	$n = 0.0$			$n = 0.0$		
0.5	1.896726	0.305409	1.736808	1.375964	0.206398	1.986432
1.0	2.906938	0.613401	1.646785	2.037898	0.410905	1.824643
1.5	4.037389	0.932532	1.569084	2.781046	0.622338	1.710583
2.0	5.230850	1.230850	1.497533	3.568901	0.837481	1.634643

Table 3. Variation in C_f, C_g and Nu for nanofluid (Al_2O_3) and hybrid nanofluids (Al_2O_3, Cu) against different values of K when $\Pr = 2.36$, $\mathrm{Re} = 15$, $Ha = 0.3$, $\kappa = 0.5$ and $Ec = 0.001$.

thermal gradient as on the surface grows. The effect of Pr on Newtonian fluids is close to what we're seeing in nanofluid. These characteristics are thus already retained from nanofluids.

Table 3 displays the variation in C_f, C_g and Nu for nanofluid (Al_2O_3) and hybrid nanofluids (Al_2O_3, Cu) against different estimations of K when $\Pr = 2.36$, $\mathrm{Re} = 15$, $Ha = 0.3$, $\kappa = 0.5$ and $Ec = 0.001$. The first portion is shown for the variation in C_f, C_g and Nu when $n = 0.5$. The escalating estimations of K heighten C_f and

C_g while reduce Nu for both nanofluid and hybrid nanofluid. The second portion is shown for the variation in C_f, C_g and Nu when $n = 0.0$. The escalating estimations of K heightens C_f and C_g while reduce Nu for both nanofluid and hybrid nanofluid.

Conclusion

The analytical and numerical analysis on the effect of hybrid nanoparticles (Cu and Al_2O_3) on the thermal efficiency of nano-structured nanoparticles (micropolar fluid) with Cattaneo-Christov heat flux model is discussed here. The comparison of both approaches is deliberated here as well. The main findings are as follows:

1. Continuous dispersion of Cu and Al_2O_3 leads in an optimal increase in thermal efficiency compared to single-type dispersion of nanoparticles, say Cu.
2. A continuous reduction in macro-velocity field is observed against increasing micropolar parameter and Hartmann number.
3. An opposite effect in micro-velocity field against micropolar parameter when $n = 0.5$ and $n = 0$ is observed.
4. An escalating conduct in thermal field is observed against the increasing estimations of Hartmann number, micropolar parameter, Eckert number, and material parameter while Prandtl number and thermal relaxation parameter has opposite conduct on thermal field.
5. Both the HAM and Shooting approaches are agreed with presented model and have shown quite closed comparison.

Received: 4 March 2020; Accepted: 13 October 2020
Published online: 11 January 2021

References

1. Choi, S. U. S. Enhancing thermal conductivity of fluids with nanoparticles. In *Developments and Applications of Non-Newtonian Flows, FED* Vol. 66 (eds Siginer, D. A. & Wang, H. P.) 99–105 (ASME, New York, 1995).
2. Dogonchi, A. S., Waqas, M., Seyyedi, S. M., Hashemi-Tilehnoee, M. & Ganji, D. D. CVFEM analysis for Fe_3O_4-H_2O nanofluid in an annulus subject to thermal radiation. *Int. J. Heat Mass Transfer.* **132**, 473–483 (2019).
3. Dogonchi, A. S. & Hashim. Heat transfer by natural convection of Fe_3O_4-water nanofluid in an annulus between a wavy circular cylinder and a rhombus. *Int. J. Heat Mass Transfer.* **130**, 320–332 (2019).
4. Sheikholeslami, M., Shehzad, S. A., Li, Z. & Shafee, A. Numerical modeling for alumina nanofluid magnetohydrodynamic convective heat transfer in a permeable medium using Darcy law. *Int. J. Heat Mass Transfer.* **127**, 614–622 (2018).
5. Sheikholeslami, M. & Rokni, H. B. Numerical simulation for impact of Coulomb force on nanofluid heat transfer in a porous enclosure in presence of thermal radiation. *Int. J. Heat Mass Transfer.* **118**, 823–831 (2018).
6. Safaei, M. R., Ranjbarzadeh, R., Hajizadeh, A., Bahiraei, M. & Afrand, M. Mesoscopic investigation for alumina nanofluid heat transfer in permeable medium influenced by Lorentz forces. *Int. J. Refrigeration.* **349**, 839–858 (2018).
7. Safaei, M. R. *et al.* Evaluating the effect of temperature and concentration on the thermal conductivity of ZnO-TiO_2/EG hybrid nanofluid using artificial neural network and curve fitting on experimental data. *Phys. A* **519**, 209–216 (2019).
8. Nadeem, S., Abbas, N. & Khan, A. U. Characteristics of three dimensional stagnation point flow of hybrid nanofluid past a circular cylinder. *Results Phys.* **8**, 829–835 (2018).
9. Saleem, S., Nadeem, S., Rashidi, M. M. & Raju, C. S. K. An optimal analysis of radiated nanomaterial flow with viscous dissipation and heat source. *Microsyst. Technol.* **25**, 683–689 (2019).
10. Sadiq, M. A., Khan, A. U., Saleem, S. & Nadeem, S. Numerical simulation of oscillatory oblique stagnation point flow of a magneto micropolar nanofluid. *RSC Adv.* **9**, 4751–4764 (2019).
11. Iqbal, Z., Akbar, N. S., Azhar, E. & Maraj, E. N. Performance of hybrid nanofluid (Cu-CuO/water) on MHD rotating transport in oscillating vertical channel inspired by Hall current and thermal radiation. *Alexandria Eng. J.* **57**, 1943–1954 (2018).
12. Nadeem, S. & Abbas, N. On both MHD and slip effect in micro-polar hybrid nanofluid past a circular cylinder under stagnation point region. *Can. J. Phys.* **97**, 392–399 (2019).
13. Sheikholeslami, M., Mehryan, S. A. M., Shafee, A. & Sheremet, M. A. Variable magnetic forces impact on magnetizable hybrid nanofluid heat transfer through a circular cavity. *J. Mol. Liq.* **277**, 388–396 (2019).
14. Das, R., Jana, N. & Makinde, O. D. MHD flow of Cu-Al_2O_3/water hybrid nanofluid in porous channel: Analysis of entropy generation. *Defect Diffus. Forum.* **377**, 42–61 (2017).
15. Olatundun, A. T. & Makinde, O. D. Analysis of Blasius flow of hybrid nanofluids over a convectively heated surface. *Defect Diffus. Forum.* **377**, 29–41 (2017).
16. Reddy, M. G., Rani, M. V. V. N. L. S., Kumar, K. G., Prasannakumar, B. C. & Chamkha, A. J. Cattaneo-Christov heat flux model on Blasius–Rayleigh–Stokes flow through a transitive magnetic field and Joule heating. *Phys. A* **548**, 123991 (2020).
17. Reddy, M. G., Rani, M. V. V. N. L. S., Kumar, K. G., Prasannakumar, B. C. & Lokesh, H. J. Hybrid dusty fluid flow through a Cattaneo-Christov heat flux model. *Phys. A* **551**, 123975 (2020).
18. Reddy, M. G., Rani, M. V. V. N. L. S., Kumar, K. G. & Prasannakumara, B. C. Cattaneo-Christov heat flux and non-uniform heat-source/sink impacts on radiative Oldroyd-B two-phase flow across a cone/wedge. *J Braz. Soc. Mech. Sci. Eng.* **40**, 95 (2018).
19. Shah, Z., Sheikholeslami, M., Ikramullah, & Kumamm, P. Influence of nanoparticles inclusion into water on convective magneto hydrodynamic flow with heat transfer and entropy generation through permeable domain. *Case Stud. Therm. Eng.* **21**, 100732 (2020).
20. Shah, Z., Kumam, P. & Deebani, W. Radiative MHD Casson nanofluid flow with activation energy and chemical reaction over past nonlinearly stretching surface through entropy generation. *Sci Rep.* **10**, 4402 (2020).
21. Shah, Z. *et al.* Entropy optimization and heat transfer modeling for Lorentz forces effect on solidification of NEPC. *Int. Commun. Heat Mass Transf.* **117**, 104715 (2020).
22. Eringen, A. C. Theory of micropolar fuids. *J. of Math. Mech.* **16**, 1–16 (1966).
23. Guram, G. S. & Smith, A. C. Stagnation flows of micropolar fluids with strong and weak interactions. *Comput. Math. Appl.* **6**, 213–233 (1980).
24. Gorla, R. S. R. & Takhar, H. S. Boundary layer flow of micropolar fluid on rotating axisymmetric surfaces with a concentrated heat source. *Acta Mech.* **105**, 1–10 (1994).
25. Gorla, R. S. R., Mansour, M. A. & Mohammedien, A. A. Combined convection in an axisymmetric stagnation flow of micropolar fluid. *Int. J. Numer. Methods Heat Fluid Flow* **6**, 47–55 (1996).

26. Seddeek, M. A. Flow of a magneto-micropolar fluid past a continuously moving plate. *Phys. Lett. A* **306**, 255–257 (2003).
27. Nazar, R., Amin, N., Filip, D. & Pop, I. Stagnation point flow of a micropolar fluid towards a stretching sheet. *Int. J. Non Linear Mech.* **39**, 1227–1235 (2004).
28. Takhar, H. S., Bhargava, R., Agrawal, R. S. & Balaji, A. V. S. Finite element solution of a micropolar fluid flow and heat transfer between two porous disks. *Int. J. Eng. Sci.* **38**, 1907–1922 (2000).
29. Abo-Eldahab, E. M. & Ghonaim, A. F. Radiation effects on heat transfer of a micropolar fluid through a porous medium. *Appl. Math. Comput.* **169**, 500–510 (2005).
30. Nazar, R., Amin, N. & Pop, I. Free convection boundary layer flow on an isothermal sphere in a micropolar fluid. *Int. Commun. Heat Mass Transf.* **29**, 377–386 (2002).
31. Shah, Z., Islam, S., Ayaz, H. & Khan, S. Radiative heat and mass transfer analysis of micropolar nanofluid flow of casson fluidbetween two rotating parallel plates with effects of hall current. *J. Heat Transfer.* **141**, 022401 (2019).
32. Khan, A. *et al.* Darcy-Forchheimer flow of micropolar nanofluid between two plates in the rotating frame with non-uniform heat generation/absorption. *Adv. Mech. Eng.* **10**, 1–16 (2018).
33. Tassaddiq, A. MHD flow of a fractional second grade fluid over an inclined heated plate. *Chaos Solitons Fractals.* **123**, 341–346 (2019).
34. Tassaddiq, A., Khan, I. & Nisar, K. S. Heat transfer analysis in sodium alginate based nanofluid using MoS_2 nanoparticles: Atangana-Baleanu fractional model. *Chaos Solitons Fractals.* **130**, 109445 (2020).
35. Tassaddiq, A. *et al.* Thin film flow of couple stress magneto-hydrodynamics nanofluid with convective heat over an inclined exponentially rotating stretched surface. *Coatings* **10**, 338 (2020).
36. Deebani, W., Tassaddiq, A., Shah, Z., Dawar, A. & Ali, F. Hall effect on radiative Casson fluid flow with chemical reaction on a rotating cone through entropy optimization. *Entropy.* **22**, 480 (2020).
37. Imran, N. *et al.* Influence of chemical reactions and mechanism of peristalsis for the thermal distribution obeying slip constraints: Applications to conductive transportation. *J. Mater. Res. Technol.* **9**, 6533–6543 (2020).
38. Tassaddiq, A. *et al.* Heat and mass transfer together with hybrid nanofluid flow over a rotating disk. *AIP Adv.* **10**, 55317 (2020).
39. Sohail, M., Shah, Z., Tassaddiq, A., Kumam, P. & Roy, P. Entropy generation in MHD Casson fluid flow with variable heat conductance and thermal conductivity over non-linear bi-directional stretching surface. *Sci Rep.* **10**, 12530 (2020).

Author contributions

Only one author, the submitting author prepared this manuscript.

Competing interests

The author declares no competing interests.

Additional information

Correspondence and requests for materials should be addressed to A.T.

Reprints and permissions information is available at www.nature.com/reprints.

Publisher's note Springer Nature remains neutral with regard to jurisdictional claims in published maps and institutional affiliations.